

Generation of strong magnetic fields with a laser-driven coil

Zhe Zhang¹, Baojun Zhu^{1,2}, Yutong Li^{1,2,3}, Weiman Jiang^{1,2}, Dawei Yuan⁴, Huigang Wei⁴, Guiyun Liang⁴, Feilu Wang⁴, Gang Zhao⁴, Jiayong Zhong^{3,5}, Bo Han⁵, Neng Hua⁶, Baoqiang Zhu⁶, Jianqiang Zhu⁶, Chen Wang⁷, Zhiheng Fang⁷, and Jie Zhang^{3,8}

¹Beijing National Laboratory of Condensed Matter Physics, Institute of Physics, Chinese Academy of Sciences, Beijing 100190, China

²School of Physical Sciences, University of Chinese Academy of Sciences, Beijing 100049, China

³Collaborative Innovation Center of IFSA (CICIFSA), Shanghai Jiao Tong University, Shanghai 200240, China

⁴Key Laboratory of Optical Astronomy, National Astronomical Observatories, Chinese Academy of Sciences, Beijing 100012, China

⁵Department of Astronomy, Beijing Normal University, Beijing 100875, China

⁶National Laboratory on High Power Laser and Physics, Chinese Academy of Sciences, Shanghai 201800, China

⁷Shanghai Institute of Laser Plasma, Shanghai 201800, China

⁸Key Laboratory for Laser Plasmas (MoE) and Department of Physics and Astronomy, Shanghai Jiao Tong University, Shanghai 200240, China

(Received 28 November 2017; revised 25 April 2018; accepted 9 May 2018)

Abstract

As a promising new way to generate a controllable strong magnetic field, laser-driven magnetic coils have attracted interest in many research fields. In 2013, a kilotesla level magnetic field was achieved at the Gekko XII laser facility with a capacitor–coil target. A similar approach has been adopted in a number of laboratories, with a variety of targets of different shapes. The peak strength of the magnetic field varies from a few tesla to kilotesla, with different spatio-temporal ranges. The differences are determined by the target geometry and the parameters of the incident laser. Here we present a review of the results of recent experimental studies of laser-driven magnetic field generation, as well as a discussion of the diagnostic techniques required for such rapidly changing magnetic fields. As an extension of the magnetic field generation, some applications are discussed.

Keywords: lab astrophysics; laser–plasma interaction; magnetic field; plasma astrophysics

1. Introduction

Magnetohydrodynamics (MHD) plays a fundamental role in a wide range of astrophysical phenomena, such as cooling of white dwarf stars^[1], amplification of magnetic fields (B -fields) in supernova remnants^[2], formation of solar flares^[3], filamentary structures on the sun^[4], young stellar objects^[5], accretion disks^[6], and magnetic reconnection^[7, 8]. The dynamics and stability of such astrophysical phenomena are governed by interactions between plasmas and magnetic fields, and these interactions have therefore been widely studied in laboratory experiments. Growth or suppression of hydrodynamic instabilities has been observed in plasmas in external B -fields^[9–12]. Moreover, in the context of

high-energy-density physics (HEDP), the hydrodynamical behavior of plasmas in intense B -fields is of great relevance to the development of B -assisted inertial confinement fusion^[13, 14] and fast ignition^[15–20].

In laboratory experiments, a flux density in the kilotesla region is needed to reveal the effect of B -fields under the conditions of a laser-ablated high-energy-density plasma. There are several ways to generate such strong B -fields with high-power lasers, including the important Biermann battery effect. In laser–plasma interaction, a toroidal B -field is generated along the surface of the expanded plasma, where the gradients of electron density n_e and temperature T_e are noncollinear^[21–23]:

$$\frac{\partial \mathbf{B}}{\partial t} = -\frac{1}{en_e} \nabla n_e \times \nabla T_e. \quad (1)$$

For a higher intensity laser–plasma interaction, electrons

Correspondence to: Y. Li, Beijing National Laboratory of Condensed Matter Physics, Institute of Physics, Chinese Academy of Sciences, Beijing 100190, China. Email: ytli@iphy.ac.cn

can be accelerated to relativistic velocity. The large current density of the accelerated electrons produces a spontaneous B -field surrounding the electron bunch. The strength of the B -field exceeds the kilotesla level inside solid^[24] or gaseous targets^[25, 26]. B -fields are not only directly produced by lasers, but may also be self-generated in plasma flow systems, as a sub-production of the perturbations^[27] or filamentations^[21, 28] caused by hydrodynamic instabilities. These B -fields can be further amplified to the tens of kilotesla level by plasma compression^[13, 14, 29]. Although spontaneously generated B -fields are useful in many HEDP researches, it is difficult to apply such B -fields to secondary samples, and a more easily controllable B -field in free space is essentially needed for many applications.

The use of a capacitor–coil (CC) target to generate a controllable B -field was proposed and realized on the Lekko VIII laser system by Daido *et al.*^[30] in 1986. Courtois *et al.*^[31] used a similar mechanism with a Helmholtz coil on the Vulcan laser at the Central Laser Facility in the United Kingdom and obtained a B -field of a few tesla. In 2013, Fujioka *et al.*^[32] redesigned the CC target and used it on the Gekko XII high-power laser facility. A kilotesla level B -field was achieved with a laser energy of 1.5 kJ in 1 ns^[32]. As shown in Figure 1, the target is composed of two main parts: a capacitor and a connection coil. The capacitor is formed from two metallic disks placed parallel to each other. There is a hole in the front disk that allows the laser to propagate through and focus on the rear disk. The two disks are connected by the connection coil, which generates a B -field when the discharge current flows through it.

In the past few years, laser-driven coils have been applied in many laboratories with similar targets. Some typical results with nanosecond high-power lasers are listed in Table 1, together with the results from Daido *et al.* and Courtois

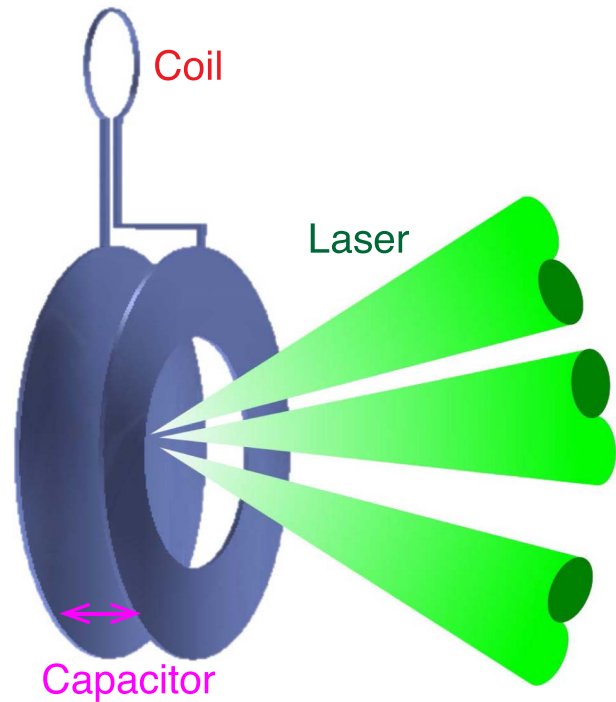


Figure 1. Basic geometry of the capacitor–coil target.

et al. for comparison. The targets used are illustrated in Figure 2. Pei *et al.*^[33] used a double-U-turn Helmholtz coil instead of a single coil to produce a counter B -field between the coils for magnetic reconnection research. Santos *et al.*^[35] modified the angle of the coil and the size of the disks to match the setting of the LULI laser facility. A U-shaped foil target was used on Omega by Goyon *et al.*^[37]. In contrast to the targets described above, Zhu *et al.*^[38] used a simpler design with only one single open-ended coil.

Table 1. Laser-driven B -fields.

Laser facility	E_{laser} (kJ)	$I\lambda^2$ ($\text{W} \cdot \text{cm}^{-2} \cdot \mu\text{m}^2$)	Target	Coil radius (mm)	B at coil center (T)	Current (kA)
Lekko VIII ^[30]	0.1	1×10^{16}	CC	1	60	100
Vulcan ^[31]	0.3	4×10^{16}	Helmholtz coil	1.25	7.5	n.a.
Gekko XII ^[32]	1.5	5×10^{16}	CC	0.25	1500 ^a	8600 ^b
Gekko XII ^[33]	1	3×10^{15}	Double-U-turn	0.3	60 ^c	82
Gekko XII ^[34]	1	2×10^{16d}	Double-CC	0.25	610	250
LULI ^[35]	0.5	1×10^{17}	CC	0.25	800	340
Omega ^[36]	1.25	2×10^{15}	CC	0.3	50	22
SG-II ^[38]	2	7×10^{14}	Single coil	0.58	200	200
Omega ^[37]	0.75	5×10^{14}	U-shape	0.25	210	180

^a B -field at 650 μm from the coil center.

^b This value could be overestimated, since the measured B -field of 1.5 kT might not result directly from the coil, and plasma compression effects could also be included.

^c B -field at 250 μm from the coil center.

^d $I\lambda^2$ of laser irradiated on each CC target.

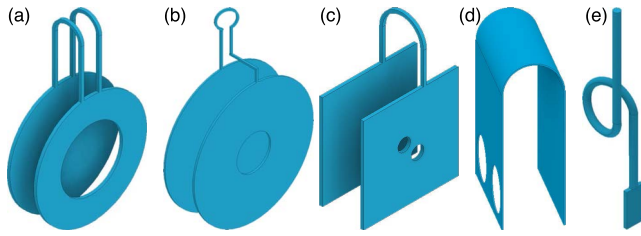


Figure 2. The illustration of targets used in (a) Ref. [33], (b) Ref. [35], (c) Ref. [36], (d) Ref. [37], and (e) Ref. [38].

2. Generation of the B -field

The main mechanism of laser-driven B -field generation involves two steps: establishment of an electrical potential and, as a consequence, generation of a B -field by the driven current.

2.1. Establishment of a potential with the laser

First, when a laser pulse irradiates a disk, some electrons are heated. Suprathermal electrons escape from the disk surface, and a potential barrier is created^[39, 40]. This barrier potential pulls back a fraction of the escaping electrons and, at the same time, induces a return current inside the target to neutralize the charge. In comparison with a single open-ended coil^[38], the front disk on the CC target captures a proportion of the escaping electrons, thereby enhancing the potential.

The initial potential is dominated by the effect of the irradiating laser, although it is also affected by the disk material. To increase the initial potential, it is necessary to increase the number of escaping electrons. The number of escaping electrons, and thus their total charge, is determined by both the suprathermal electron temperature T_e and the barrier potential V_b . Considering a simple model and assuming a static barrier potential of V_b , only electrons with an energy greater than qV_b can escape from the target surface. Assuming an energy distribution for the suprathermal electrons with an exponential high-energy tail of the form

$$f(E) = \frac{1}{T_e} \exp(-E/T_e), \quad (2)$$

the total number of electrons N_{tot} and the number of electrons that escape N_{esc} can be estimated as

$$N_{\text{tot}} = \frac{E_{\text{laser}}\eta}{T_e}, \quad (3)$$

$$N_{\text{esc}} = N_{\text{tot}} \int_{V_b}^{\infty} f(E) dE, \quad (4)$$

respectively, where E_{laser} is the laser energy and η is the absorption fraction. For unit laser energy at constant absorption, the number of escaping electrons per unit laser energy

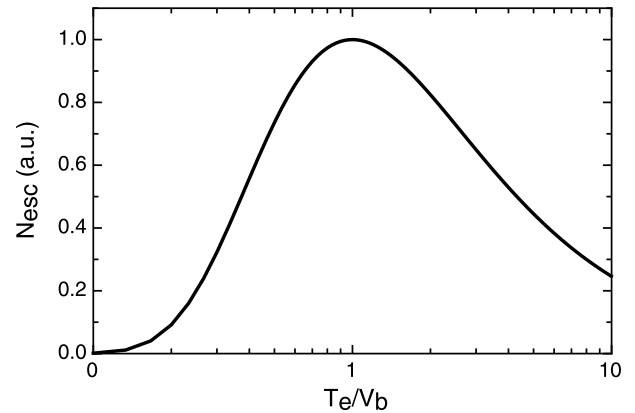


Figure 3. The number of escaping electrons per unit laser energy as a function of T_e/V_b .

is plotted in Figure 3 as a function of T_e normalized by the barrier potential V_b . The number of escaping electrons reaches a maximum value when T_e is equal to V_b . The existence of an optimal T_e can be understood as the result of competition between the suprathermal electrons and the escaping fraction. With a higher T_e , more electrons exceed the barrier potential and escape from the target surface, and, with a fixed absorption of laser energy, the total number of suprathermal electrons is decreased. Since T_e is related to the laser irradiance $I\lambda^2$, it is possible, for a known absorption mechanism, to find the optimal incident laser parameters to maximize the potential. However, the laser absorption η depends on the laser irradiance, and V_b is strongly dependent on electron heating and escape, so more sophisticated models are needed to provide more realistic solutions. However, this discussion is beyond the scope of this article.

2.2. Generation of the B -field

With the establishment of an initial potential V_0 between the two disks, the target behaves toward the potential like a resistor–inductor (RL) electrical circuit. The time evolution of the current $I(t)$ can be treated using an RL model:

$$V_0(t) = L \frac{dI(t)}{dt} + RI(t), \quad (5)$$

where L and R are the inductance and resistance, respectively. For the targets illustrated in Figure 2, the resistance is usually negligibly small compared with the inductance. Reducing the inductance by reshaping the coil could result in a higher peak current. However, we should also note that the coil shape also determines the spatio-temporal ranges of the B -field. An appropriate balance should be found between the peak strength and distribution of the B -field, depending on the intended application.

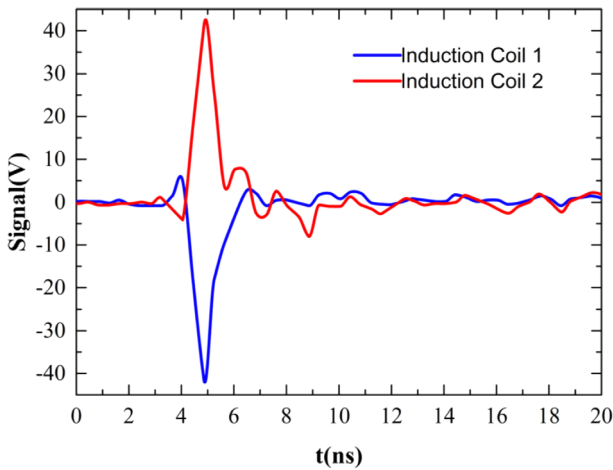


Figure 4. Typical symmetric signal observed with a differential twisted pair^[38].

2.3. Discussion

The B -field, generated by the potential V_0 and the current in the coil $I(t)$, is controlled by both the incident laser and the shape of the target. For example, from a comparison of the results of Daido *et al.*^[30] and Fujioka *et al.*^[32], it can be seen that although similar target geometries were applied, the strength of the B -field was increased over 25 times by increasing the laser energy by a factor of 15. Furthermore, although the use of a Helmholtz coil by Courtois *et al.*^[31] dramatically increased the inductance and thus decreased the peak B -field, the duration of the field was increased compared with the case of a single coil, and much better spatial uniformity was achieved. Thus, it is necessary to consider not only the peak strength of the B -field, but also its temporal evolution and spatial distribution.

As well as those mentioned in the above discussion, some other models have been proposed for the study of laser-driven B -fields^[41–43].

3. Measurement of the B -field

3.1. B -dot probe

A rapidly changing B -field can be measured in many ways. One traditional method uses a pick-up coil, also known as a B -dot probe. The basic idea is to utilize Faraday's law to measure B -field fluctuations dB/dt ^[44]. However, B -dot measurements usually suffer from strong electromagnetic pulse noise from laser–plasma interactions, and it is therefore necessary to adopt techniques that can distinguish between the signal from the magnetic coil and that from laser–plasma interactions. First of all, for a single B -dot probe, the probe should consist of a differentially twisted pair so that symmetric signals then indicate a B -field, while asymmetric signals

might be caused by heating of the probe by high-energy particles or X-rays. Figure 4 shows a typical signal obtained by Zhu *et al.*^[38], in which two symmetric pulses from the differential pair can be clearly seen. Other approaches to alleviating the noise problem involve placing multiple B -dot probes at different positions or using a multidimensional B -dot probe that detects the B -field along three orthogonal axes at the same point^[45]. Since the B -field generated from a laser-driven coil is strongly directional, while the noise from laser–plasma interactions is relatively isotropic, the B -field from the coil can be extracted by comparing signals at different points or from different directions. One disadvantage of the B -dot probe concerns bandwidth. For a B -field driven by a picosecond or femtosecond laser, the rise time can be at a picosecond scale, so the bandwidth of the B -dot probe and that of the oscilloscope need to be very high to evaluate the peak of the B -field, and this is very hard to achieve.

3.2. Optical probe

Another approach to measuring the B -field involves the use of an optical diagnostic technique, such as that based on the Faraday effect. The Faraday effect is a magneto-optical phenomenon in which, when polarized light propagates through a magneto-optical medium in a B -field, the plane of polarization is rotated, with the angle of rotation being proportional to the strength of the B -field in the direction of propagation:

$$\Delta\theta = LV B_L, \quad (6)$$

where L is the length of the optical path, V is the Verdet constant, and B_L is the component of the B -field parallel to the direction of propagation of the probe laser beam. Such a method was applied using a SiO_2 crystal by Fujioka *et al.*^[32] and later using a terbium gallium garnet by Santos *et al.*^[35]. Both experiments used a streak camera as the detector to obtain measurements with high temporal resolution. A typical setup for a Faraday effect measurement is shown in Figure 5(a). A Faraday crystal is positioned beside the magnetic coil, with a linearly polarized probe laser beam propagating through it. On applying the B -field generated by the coil to the crystal, the plane of polarization is rotated. By means of a Wollaston prism, the probe beam is divided into two orthogonal linearly polarized components. Both outgoing beams are imaged on the slit of a streak camera to measure the temporal evolution. An example from Ref. [32] is shown in Figures 5(b) and 5(c). A reference image was taken without a B -field driven laser. The probe beam was horizontally polarized and appeared only on the right side of the image. With a laser-driven B -field, the plane of polarization was rotated, with the vertically polarized component appearing on the left side. The angle of rotation

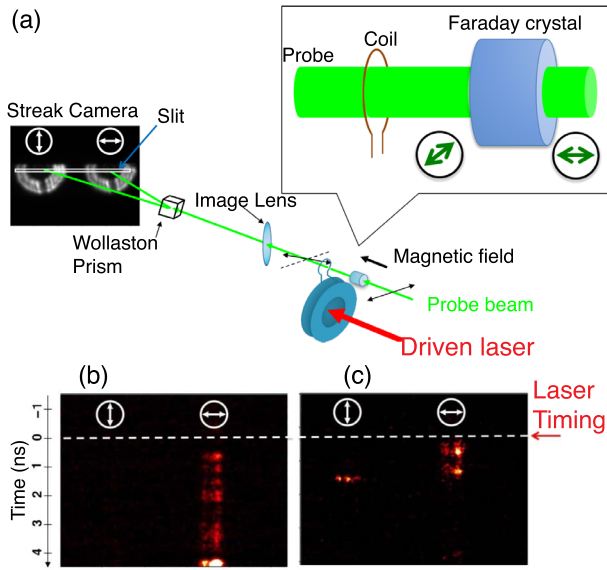


Figure 5. Example of a Faraday rotation measurement: (a) typical setup; (b) reference image; (c) image in the presence of a B -field^[32].

$\Delta\theta$ can then be estimated from the change in the intensity ratio for both polarization components as follows:

$$R = \frac{I_{\text{left}}}{I_{\text{left}} + I_{\text{right}}}, \quad (7)$$

$$\sin^2(\theta + \Delta\theta) - \sin^2\theta = \Delta R, \quad (8)$$

where I_{left} and I_{right} are the intensities of the probe beam read from the streak camera. The strength of the B -field can be then estimated from the value of $\Delta\theta$, using Equation (6).

Another approach applies the Cotton–Mouton effect, which occurs when a Cotton–Mouton medium is subjected to a B -field^[46, 47]. A linearly polarized probe laser beam becomes elliptically polarized owing to the Cotton–Mouton effect, and, by measuring the ellipticity β , the B -field can be estimated by solving the equation

$$\beta = \frac{e^2}{m_e c^3 \omega n_c} \int n_e(l) B^2(l) dl, \quad (9)$$

where l is the path length traversed by the probe laser beam inside the plasma. In contrast to the Faraday effect, the Cotton–Mouton effect detects the B -field perpendicular to the direction of propagation of the probe beam.

Additional measurements of the plasma profile, especially the electron density profile $n_e(l)$, are essential for accurate evaluation of the B -field strength.

3.3. Charged-particle deflectometry

With the target normal sheath acceleration (TNSA), it is easy to obtain high-energy proton beams with a cutoff

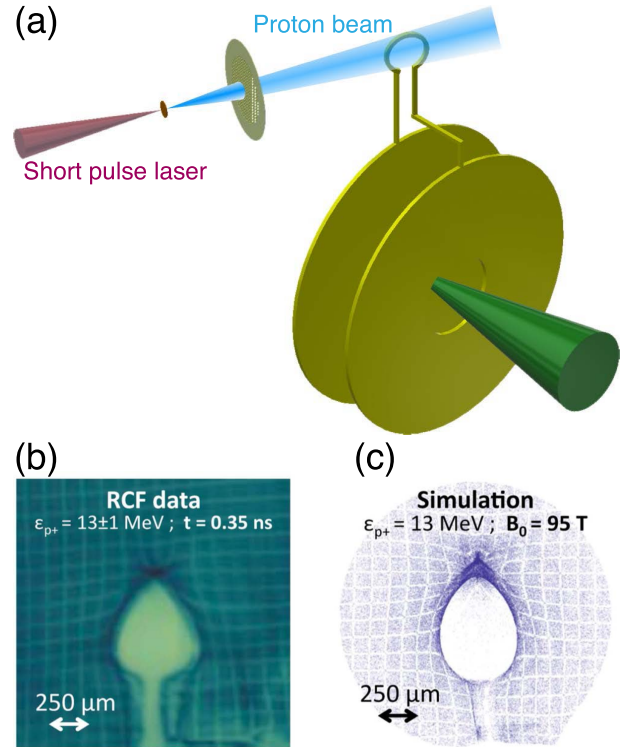


Figure 6. Example of a proton deflectometry measurement: (a) schematic of the setup; (b) image obtained on RCF with 13 MeV protons; (c) simulation of proton deflection in a B -field^[35].

energy of tens of MeV^[48, 49]. An alternative is to generate a monoenergetic proton beam as a product of nuclear fusion^[23]. The protons are deflected by the Lorentz force while propagating through the magnetic coil region. An example of an experimental setting used by Santos *et al.*^[35] is shown in Figure 6(a). The experiments were conducted at the LULI Pico 2000 laser facility with synchronized nanosecond and picosecond laser pulses. The nanosecond laser beam was focused on a CC target to generate a B -field in the coil. A secondary target was positioned beside the coil, and TNSA proton beams directed toward the coil were driven by the picosecond laser. A mesh was placed between the secondary target and the coil to quantify the B -field. Figure 6(b) shows an image of proton deflectometry achieved with 13 MeV protons. The deformation of the mesh shadow and a bulb shape at the coil can be clearly seen. Figure 6(c) shows the result of a three-dimensional Monte Carlo simulation of the trajectories of 13 MeV protons through the coil. By comparing the experimentally obtained proton image with the simulation results, information about the B -field can be derived. Proton deflectometry allows direct measurement of the B -field in the coil region, with spatial and temporal resolutions being obtained in a single shot. The spatial resolution is found by recording a two-dimensional deflection pattern with radiochromic film (RCF)

stacks. Protons are stopped at different layers in the RCF, with each layer corresponding to a specific proton energy. By taking into account the time of flight between the proton source and the coil, the pattern on each RCF layer represents the B -field at different times. Evaluations of the strength of a laser-driven B -field using proton deflectometry have been reported previously by Li *et al.*^[23, 50] and have been applied on a coil target by Santos *et al.*^[35], Zhu *et al.*^[38], Gao *et al.*^[36], Law *et al.*^[34] and Goyon *et al.*^[37].

As well as protons, high-energy electrons can be employed in deflectometry measurements. The energies of laser wake-field accelerated electrons can reach hundreds of MeV and even the GeV level^[51], and, under particular conditions, a monoenergetic electron beam can be obtained^[52]. Such electron beams provide a powerful diagnostic tool for B -fields. The Larmor radius for a relativistic electron in the presence of a B -field is

$$r_L = \frac{\gamma m_e v_\perp}{qB}, \quad (10)$$

where γ , m_e , v_\perp and q are the Lorentz factor, electron mass, component of velocity perpendicular to the B -field and electron charge, respectively. The minimum requirement for the electron energy can be approximately estimated by limiting the region of nonzero B -field, of dimension R , to be smaller than r_L . In Figure 7, the minimum electron energy is shown as a function of the product of B -field strength and the extent of the B -field, $B \cdot R$ in units of T-mm. As expected, to measure a large B -field with a large spatial range, a higher electron energy is needed.

4. Applications

We present here some typical applications of laser-driven coils to generate strong B -fields for laboratory studies.

4.1. Low- β magnetic reconnection

Magnetic reconnection is an important process in many astrophysical phenomena, including solar flares, star formation and auroras, and there have been a number of laboratory investigations based on laser-plasma interactions^[7, 8]. To mimic the conditions of low- β magnetic reconnection (where β is the ratio of plasma pressure to magnetic pressure), it is necessary to apply a B -field to a low-density plasma. Pei *et al.*^[33] used a double-U-turn coil for this purpose, with an antiparallel B -field being generated between the two coils. Heating by the current in the coil and by X-rays from the laser ablation leads to the creation of a low-density plasma, which then flows into the B -field. Low- β magnetic reconnection can occur under these conditions.

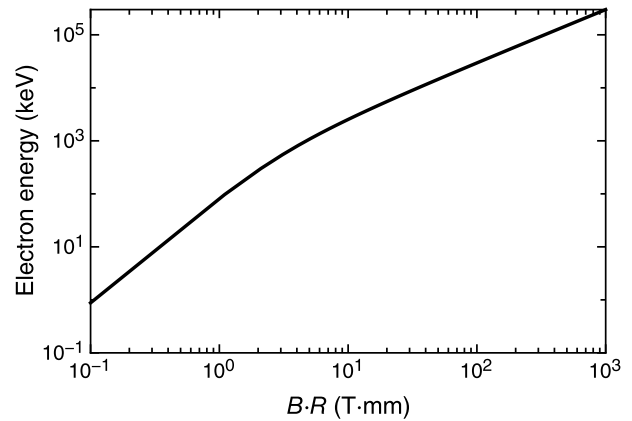


Figure 7. Minimum electron energy required for electron deflectometry, as a function of the product $B \cdot R$.

4.2. Collimation of relativistic electron beams

A collimated relativistic electron beam (REB) is useful for many applications, but the REBs produced by intense laser interaction with a solid target are usually strongly divergent. Simulations have shown that a kilotesla external B -field could effectively decrease the angle of divergence of the REB^[16]. Such collimated REBs have been experimentally investigated by Bailly-Grandvaux *et al.*^[20].

4.3. MHD

Matsuo *et al.*^[12] applied a pair of CC targets to generate a quasi-uniform B -field of a few hundred tesla in a laser-produced plasma. By adding a secondary laser-ablated sample in the B -field, the MHD properties of the plasma were studied. Electron thermal conduction in the external B -field was found to be strongly affected, leading to velocity changes in the ablated plasma. The results also indicated that the growth of hydrodynamic perturbations was also affected by the external B -field as a result of the anisotropic thermal conductivity in the ablated plasma.

5. Conclusions

The use of laser-driven coils is an important method to provide a strong B -field at a sub-kilotesla to a kilotesla level. In addition to the high field strength achievable, the controllability of generation and accessibility of a secondary sample are other advantages of this scheme. The strength, space and time ranges of the B -field could be further optimized depending on the desired application through appropriate choices of incident laser, target and coil shapes. This scheme could provide a new test bed for a range of laboratory applications including, but not limited to, HEDP, laboratory astrophysics, fusion research and laser particle acceleration.

Many types of target have been tested under different laser conditions. There are also some other advanced designs for generation of strong B -fields using short-pulse lasers, such as the snail-shaped target proposed by Korneev *et al.*^[53].

Acknowledgements

This study was supported in part by the Science Challenge Project (No. TZ2016005), the CAS-JSPS Joint Research Program (External Cooperation Program of the BIC, Chinese Academy of Sciences, No. 112111KYSB20160015), the National Natural Science Foundation of China (Nos. 11520101003, 11535001 and 11861121001) and the Strategic Priority Research Program of the Chinese Academy of Sciences (Nos. XDB16010200 and XDB07030300).

References

- G. Valyavin, D. Shulyak, G. A. Wade, K. Antonyuk, S. V. Zharikov, G. A. Galazutdinov, S. Plachinda, S. Bagnulo, L. F. Machado, M. Alvarez, D. M. Clark, J. M. Lopez, D. Hiriart, I. Han, Y.-B. Jeon, C. Zurita, R. Mujica, T. Burlakova, T. Szeifert, and A. Burenkov, *Nature* **515**, 88 (2014).
- J. Meinecke, H. W. Doyle, F. Miniati, A. R. Bell, R. Bingham, R. Crowston, R. P. Drake, M. Fatenejad, M. Koenig, Y. Kuramitsu, C. C. Kuranz, D. Q. Lamb, D. Lee, M. J. MacDonald, C. D. Murphy, H. S. Park, A. Pelka, A. Ravasio, Y. Sakawa, A. A. Schekochihin, A. Scopatz, P. Tzeferacos, W. C. Wan, N. C. Woolsey, R. Yurchak, B. Reville, and G. Gregori, *Nat. Phys.* **10**, 520 (2014).
- S. Masuda, T. Kosugi, H. Hara, S. Tsuneta, and Y. Ogawara, *Nature* **371**, 495 (1994).
- H. Isobe, T. Miyagoshi, K. Shibata, and T. Yokoyama, *Nature* **434**, 478 (2005).
- B. Albertazzi, A. Ciardi, M. Nakatsutsumi, T. Vinci, J. Beard, R. Bonito, J. Billette, M. Borghesi, Z. Burkley, S. N. Chen, T. E. Cowan, T. Herrmannsdorfer, D. P. Higginson, F. Kroll, S. A. Pikuz, K. Naughton, L. Romagnani, C. Riconda, G. Revet, R. Riquier, H. P. Schlenvoigt, I. Y. Skobelev, A. Y. Faenov, A. Soloviev, M. Huarte-Espinosa, A. Frank, O. Portugall, H. Pepin, and J. Fuchs, *Science* **346**, 325 (2014).
- S. A. Balbus and J. F. Hawley, *Astrophys. J.* **376**, 214 (1991).
- P. M. Nilson, L. Willingale, M. C. Kaluza, C. Kamperidis, S. Minardi, M. S. Wei, P. Fernandes, M. Notley, S. Bandyopadhyay, M. Sherlock, R. J. Kingham, M. Tatarakis, Z. Najmudin, W. Rozmus, R. G. Evans, M. G. Haines, A. E. Dangor, and K. Krushelnick, *Phys. Rev. Lett.* **97**, 255001 (2006).
- J. Y. Zhong, Y. T. Li, X. Wang, J. Wang, Q. Dong, C. Xiao, S. J. Wang, X. Liu, L. Zhang, L. An, F. Wang, J. Zhu, Y. Gu, X. He, G. Zhao, and J. Zhang, *Nat. Phys.* **6**, 984 (2010).
- Y. Sentoku, K. Mima, S. I. Kojima, and H. Ruhl, *Phys. Plasmas* **7**, 689 (2000).
- J. M. Stone and T. Gardiner, *Astrophys. J.* **671**, 1726 (2007).
- T. Sano, T. Inoue, and K. Nishihara, *Phys. Rev. Lett.* **111**, 205001 (2013).
- K. Matsuo, H. Nagatomo, Z. Zhang, P. Nicolai, T. Sano, S. Sakata, S. Kojima, S. H. Lee, K. F. F. Law, Y. Arikawa, Y. Sakawa, T. Morita, Y. Kuramitsu, S. Fujioka, and H. Azechi, *Phys. Rev. E* **95**, 053204 (2017).
- P. Y. Chang, G. Fiksel, M. Hohenberger, J. P. Knauer, R. Betti, F. J. Marshall, D. D. Meyerhofer, F. H. Seguin, and R. D. Petrasso, *Phys. Rev. Lett.* **107**, 035006 (2011).
- M. Hohenberger, P. Y. Chang, G. Fiksel, J. P. Knauer, R. Betti, F. J. Marshall, D. D. Meyerhofer, F. H. Seguin, and R. D. Petrasso, *Phys. Plasmas* **19**, 056306 (2012).
- H. Nagatomo, T. Johzaki, A. Sunahara, H. Sakagami, K. Mima, H. Shiraga, and H. Azechi, *Nucl. Fusion* **53**, 063018 (2013).
- H. B. Cai, S. P. Zhu, and X. T. He, *Phys. Plasmas* **20**, 072701 (2013).
- W. M. Wang, P. Gibbon, Z. M. Sheng, and Y. T. Li, *Phys. Rev. Lett.* **114**, 015001 (2015).
- S. Fujioka, Y. Arikawa, S. Kojima, T. Johzaki, H. Nagatomo, H. Sawada, S. H. Lee, T. Shiroto, N. Ohnishi, A. Morace, X. Vaisseau, S. Sakata, Y. Abe, K. Matsuo, K. F. Farley Law, S. Tosaki, A. Yogo, K. Shigemori, Y. Hironaka, Z. Zhang, A. Sunahara, T. Ozaki, H. Sakagami, K. Mima, Y. Fujimoto, K. Yamanoi, T. Norimatsu, S. Tokita, Y. Nakata, J. Kawanaka, T. Jitsuno, N. Miyanaga, M. Nakai, H. Nishimura, H. Shiraga, K. Kondo, M. Bailly-Grandvaux, C. Bellei, J. J. Santos, and H. Azechi, *Phys. Plasmas* **23**, 056308 (2016).
- T. Johzaki, H. Nagatomo, A. Sunahara, Y. Sentoku, H. Sakagami, M. Hata, T. Taguchi, K. Mima, Y. Kai, D. Ajimi, T. Isoda, T. Endo, A. Yogo, Y. Arikawa, S. Fujioka, H. Shiraga, and H. Azechi, *Plasma Phys. Control. Fusion* **59**, 014045 (2016).
- M. Bailly-Grandvaux, J. J. Santos, C. Bellei, P. Forestier-Colleoni, S. Fujioka, L. Giuffrida, J. J. Honrubia, D. Batani, R. Bouillaud, M. Chevrot, J. E. Cross, R. Crowston, S. Dorard, J.-L. Dubois, M. Ehret, G. Gregori, S. Hulin, S. Kojima, E. Loyez, J.-R. Marquès, A. Morace, P. Nicolai, M. Roth, S. Sakata, G. Schaumann, F. Serres, J. Servel, V. T. Tikhonchuk, N. Woolsey, and Z. Zhang, *Nat. Commun.* **9**, 102 (2017).
- K. M. Schoeffler, N. F. Loureiro, R. A. Fonseca, and L. O. Silva, *Phys. Plasmas* **23**, 056304 (2016).
- L. Gao, P. M. Nilson, I. V. Igumenshchev, M. G. Haines, D. H. Froula, R. Betti, and D. D. Meyerhofer, *Phys. Rev. Lett.* **114**, 215003 (2015).
- C. K. Li, F. H. Seguin, J. A. Frenje, J. R. Rygg, R. D. Petrasso, R. P. J. Town, P. A. Amendt, S. P. Hatchett, O. L. Landen, A. J. MacKinnon, P. K. Patel, V. A. Smalyuk, T. C. Sangster, and J. P. Knauer, *Phys. Rev. Lett.* **97**, 135003 (2006).
- S. Chawla, M. S. Wei, R. Mishra, K. U. Akli, C. D. Chen, H. S. McLean, A. Morace, P. K. Patel, H. Sawada, Y. Sentoku, R. B. Stephens, and F. N. Beg, *Phys. Rev. Lett.* **110**, 025001 (2013).
- A. G. Smyth, G. Sarri, M. Vranic, Y. Amano, D. Doria, E. Guillaume, H. Habara, R. Heathcote, G. Hicks, Z. Najmudin, H. Nakamura, P. A. Norreys, S. Kar, L. O. Silva, K. A. Tanaka, J. Vieira, and M. Borghesi, *Phys. Plasmas* **23**, 063121 (2016).
- W. Schumaker, N. Nakanii, C. McGuffey, C. Zulick, V. Chyvkov, F. Dollar, H. Habara, G. Kalintchenko, A. Maksimchuk, K. A. Tanaka, A. G. R. Thomas, V. Yanovsky, and K. Krushelnick, *Phys. Rev. Lett.* **110**, 015003 (2013).
- M. J. E. Manuel, C. K. Li, F. H. Seguin, J. Frenje, D. T. Casey, R. D. Petrasso, S. X. Hu, R. Betti, J. D. Hager, D. D. Meyerhofer, and V. A. Smalyuk, *Phys. Rev. Lett.* **108**, 255006 (2012).
- C. M. Huntington, F. Fiuza, J. S. Ross, A. B. Zylstra, R. P. Drake, D. H. Froula, G. Gregori, N. L. Kugland, C. C. Kuranz, M. C. Levy, C. K. Li, J. Meinecke, T. Morita, R. Petrasso, C. Plechaty, B. A. Remington, D. D. Ryutov, Y. Sakawa, A. Spitkovsky, H. Takabe, and H. S. Park, *Nat. Phys.* **11**, 173 (2015).

29. J. P. Knauer, O. V. Gotchev, P. Y. Chang, D. D. Meyerhofer, O. Polomarov, R. Betti, J. A. Frenje, C. K. Li, M. J. E. Manuel, R. D. Petrasso, J. R. Rygg, and F. H. Seguin, *Phys. Plasmas* **17**, 056318 (2010).
30. H. Daido, F. Miki, K. Mima, M. Fujita, K. Sawai, and H. Fujita, *Phys. Rev. Lett.* **56**, 846 (1986).
31. C. Courtois, A. D. Ash, D. M. Chambers, R. A. D. Grundy, and N. C. Woolsey, *J. Appl. Phys.* **98**, 054913 (2005).
32. S. Fujioka, Z. Zhang, K. Ishihara, K. Shigemori, Y. Hironaka, T. Johzaki, A. Sunahara, N. Yamamoto, H. Nakashima, T. Watanabe, H. Shiraga, H. Nishimura, and H. Azechi, *Sci. Rep.* **3**, 1170 (2013).
33. X. X. Pei, J. Y. Zhong, Y. Sakawa, Z. Zhang, K. Zhang, H. G. Wei, Y. T. Li, Y. F. Li, B. J. Zhu, T. Sano, Y. Hara, S. Kondo, S. Fujioka, G. Y. Liang, F. L. Wang, and G. Zhao, *Phys. Plasmas* **23**, 032125 (2016).
34. K. F. F. Law, M. Bailly-Grandvaux, A. Morace, S. Sakata, K. Matsuo, S. Kojima, S. Lee, X. Vaisseau, Y. Arikawa, A. Yogo, K. Kondo, Z. Zhang, C. Bellei, J. J. Santos, S. Fujioka, and H. Azechi, *Appl. Phys. Lett.* **108**, 091104 (2016).
35. J. J. Santos, M. Bailly-Grandvaux, L. Giuffrida, P. Forestier-Colleoni, S. Fujioka, Z. Zhang, P. Korneev, R. Bouillaud, S. Dorard, D. Batani, M. Chevrot, J. E. Cross, R. Crowston, J.-L. Dubois, J. Gazave, G. Gregori, E. D'Humières, S. Hulin, K. Ishihara, S. Kojima, E. Loyez, J.-R. Marquès, A. Morace, P. Nicolai, O. Peyrusse, A. Poyé, D. Raffestin, J. Ribolzi, M. Roth, G. Schaumann, F. Serres, V. T. Tikhonchuk, P. Vacar, and N. Woolsey, *New J. Phys.* **17**, 083051 (2015).
36. L. Gao, H. Ji, G. Fiksel, W. Fox, M. Evans, and N. Alfonso, *Phys. Plasmas* **23**, 043106 (2016).
37. C. Goyon, B. B. Pollock, D. P. Turnbull, A. Hazi, L. Divol, W. A. Farmer, D. Haberberger, J. Javedani, A. J. Johnson, A. Kemp, M. C. Levy, B. Grant Logan, D. A. Mariscal, O. L. Landen, S. Patankar, J. S. Ross, A. M. Rubenchik, G. F. Swadling, G. J. Williams, S. Fujioka, K. F. F. Law, and J. D. Moody, *Phys. Rev. E* **95**, 474 (2017).
38. B. J. Zhu, Y. T. Li, D. W. Yuan, Y. F. Li, F. Li, G. Q. Liao, J. R. Zhao, J. Y. Zhong, F. B. Xue, S. K. He, W. M. Wang, F. Lu, F. Q. Zhang, L. Yang, K. N. Zhou, N. Xie, W. Hong, H. G. Wei, K. Zhang, B. Han, X. X. Pei, C. Liu, Z. Zhang, J. Q. Zhu, Y. Gu, Z. Q. Zhao, B. H. Zhang, G. Zhao, and J. Zhang, *Appl. Phys. Lett.* **107**, 261903 (2015).
39. A. Poyé, J.-L. Dubois, F. Lubrano-Lavaderci, E. D'Humières, M. Bardou, S. Hulin, M. Bailly-Grandvaux, J. Ribolzi, D. Raffestin, J. J. Santos, P. Nicolai, and V. Tikhonchuk, *Phys. Rev. E* **92**, 043107 (2015).
40. J.-L. Dubois, F. Lubrano-Lavaderci, D. Raffestin, J. Ribolzi, J. Gazave, A. C. L. Fontaine, E. D'Humières, S. Hulin, P. Nicola, A. Poyé, and V. T. Tikhonchuk, *Phys. Rev. E* **89**, 68 (2014).
41. G. Fiksel, W. Fox, L. Gao, and H. Ji, *Appl. Phys. Lett.* **109**, 134103 (2016).
42. V. T. Tikhonchuk, M. Bailly-Grandvaux, J. J. Santos, and A. Poyé, *Phys. Rev. E* **96**, 474 (2017).
43. F. Schillaci, M. De Marco, L. Giuffrida, S. Fujioka, Z. Zhang, G. Korn, and D. Margarone, *AIP Adv.* **8**, 025103 (2018).
44. R. C. Phillips and E. B. Turner, *Rev. Sci. Instrum.* **36**, 1822 (1965).
45. E. T. Everson, P. Pribyl, C. G. Constantin, A. B. Zylstra, D. B. Schaeffer, N. L. Kugland, and C. Niemann, *Rev. Sci. Instrum.* **80**, 113505 (2009).
46. A. S. Sandhu, A. K. Dharmadhikari, P. P. Rajeev, G. R. Kumar, S. Sengupta, A. Das, and P. K. Kaw, *Phys. Rev. Lett.* **89**, 841 (2002).
47. M. Shaikh, A. D. Lad, K. Jana, D. Sarkar, I. Dey, and G. R. Kumar, *Plasma Phys. Control. Fusion* **59**, 014007 (2016).
48. S. C. Wilks, A. B. Langdon, T. E. Cowan, M. Roth, M. Singh, S. Hatchett, M. H. Key, D. Pennington, A. MacKinnon, and R. A. Snavely, *Phys. Plasmas* **8**, 542 (2001).
49. M. Passoni, L. Bertagna, and A. Zani, *New J. Phys.* **12**, 045012 (2010).
50. C. K. Li, F. H. Seguin, J. A. Frenje, M. Rosenberg, R. D. Petrasso, P. A. Amendt, J. A. Koch, O. L. Landen, H. S. Park, H. F. Robey, R. P. J. Town, A. Casner, F. Philippe, R. Betti, J. P. Knauer, D. D. Meyerhofer, C. A. Back, J. D. Kilkenny, and A. Nikroo, *Science* **327**, 1231 (2010).
51. M. Mirzaie, S. Li, M. Zeng, N. A. M. Hafz, M. Chen, G. Y. Li, Q. J. Zhu, H. Liao, T. Sokollik, F. Liu, Y. Y. Ma, L. M. Chen, Z. M. Sheng, and J. Zhang, *Sci. Rep.* **5**, 14659 (2015).
52. S. Mangles, C. D. Murphy, Z. Najmudin, and A. Thomas, *Nature* **43**, 535 (2004).
53. P. Korneev, E. D'Humières, and V. Tikhonchuk, *Phys. Rev. E* **91**, 043107 (2015).